ITC 4/54
Information Technology and Control
Vol. 54 / No. 4/ 2025
pp. 1343-1357
DOI 10.5755/j01.itc.54.4.40174

Modified Super-Twisting Sliding Mode Speed Controller for Predictive Control of Induction Motor

Received 2025/01/14 | Accepted after revision 2025/06/26

HOW TO CITE: Vo H. H., Dong, C. S. T., Vo, D. H., Brandstetter P. (2025). Modified Super-Twisting Sliding Mode Speed Controller for Predictive Control of Induction Motor. *Information Technology and Control*, 54(4), 1343-1357. https://doi.org/10.5755/j01.itc.54.4.40174

Modified Super-Twisting Sliding Mode Speed Controller for Predictive Control of Induction Motor

Hau H. Vo*, Chau S. T. Dong, Duy H. Vo

Modeling Evolutionary Algorithms Simulation and Artificial Intelligence, Faculty of Electrical and Electronics Engineering; Ton Duc Thang University; No. 19 Nguyen Huu Tho Street, Tan Hung Ward, Ho Chi Minh City, Vietnam; phone: + 84 28 3775 5028; fax: + 84 28 3775 5055; e-mails: vohuuhau@tdtu.edu.vn, dongsithienchau@tdtu.edu.vn, vohoangduy@tdtu.edu.vn

Pavel Brandstetter

Department of Applied Electronics, Faculty of Electrical Engineering and Computer Science; VSB-Technical University of Ostrava; 17. listopadu 15, 70833 Ostrava-Poruba, Czech Republic; phone: +420 597 326 001; fax: + 420 596 919 597; e-mail: pavel.brandstetter@vsb.cz

Corresponding author: vohuuhau@tdtu.edu.vn

The paper deals with modification of super-twisting algorithm in sliding mode speed controller for predictive control of induction motor. In the challenging operating regions of the induction motor including very-low speed and/or high-load torque, the conventional proportional-integral (PI) controller gives undesirable speed response performance. In order to enhance the performance, sliding mode control (SMC) is deployed. However, the conventional SMC often owns high-chattering control signal. In order to simultaneously reduce the chattering phenomenon and achieve high accuracy of the speed response, super-twisting algorithm-based control law that is adapted according to sign of time derivative of disturbance, is utilized. Additionally, boundaries of the disturbance term and its time derivative are defined using dynamic equation of the motor and the prediction process. Simulations with the predictive control of three controllers confirm the superior performance of the proposed super-twisting algorithm in terms of normalized integral time absolute error and relative final error of the motor speed compared to the PI and the conventional SMC ones.

KEYWORDS: Induction Motor, Predictive Control, Speed Controller, Sliding Mode Control (SMC), Super-Twisting Algorithm

1. Introduction

Predictive control (PC) has been deploying in applications of power electronics and electrical drives. To lower ripple of linear induction motors (IMs), a model PC was utilized [9]. The PC using loss model was employed to optimize the IM efficiency [15]. The conventional proportional-integral (PI) current controller was replaced by a PC-based one for improving charateristics performance [22]. To reduce power losses and keep performance of output current, a model PC was applied for power converters [23]. The simplified PC for the IM gave the drive characteristics comparable to direct torque control [29]. The deadbeat method increased the robustness of the PC of the IM current [33]. The PC approach utilizing phase lock loop analysis maintained control stability of an inverter [36]. The constant frequency PC improved the steady-state IM response [45]. For robust system control, many approaches were applied.

End-effects and loss were added into the design of feedback linearization controller to improve the system performance [1]. The backstepping method was utilized in accurate control of eletric vehicles driven by direct torque controlled doubly fed IM [6]. The advantages of population-based optimization algorithm and field programmable gate array reduced computing demands of a nonlinear PC approach significantly [18]. In the PMSM drive, a performance boundary function was integrated in a funnel-like function to handle the constraints [21]. The complexity of the backstepping was also minimized by command filtering and a compensating-based error reduction. The linear permanent magnet synchronous motor (PMSM) model was obtained by direct torque control (DTC) utilizing feedback linearization [24]. The Taylor series expansion was used to linearize the 5-phase IM, and an H-infininity-based controller utilized the linearized model to control the system optimally [31]. To avoid high computation requirement, the backstepping synchronization control integrated the filtering, the compensation of the unknown dynamics and disturbances using the adaptive control for a servo drive system [39]. A two-step input disturbance estimation and a robust feedback controller utilizing linear matrix inequalities enhanced the mechatronic system performance [40]. A trajectory planning approach utilizing model-free reinforcement learning technique was deployed for a high-underactuation pendulum crane driven by an IM whose model was identified [41]. A multilayer artificial neural network was employed to reject both matched and mismatched disturbances and compensate both exogenous and endogenous ones for high-performance control of highly uncertain nonlinear systems [43]. A control architecture using state filtered disturbance rejection and backstepping method for compensating the lumped disturbances and eliminating the complexity, was presented to improve the control performance [44]. To obtain high-performance control, the described methods require complicated design process. Among robust control techniques, sliding mode control (SMC) is a commonly-used one.

The SMC was employed for sensorless control at high and medium speed regions [3]. Both speed controller and speed observer were enhanced by the SMC [7]. A non-singular terminal SMC brought finite time convergence in the disturbed and uncertain rehabilitation system [12]. Active disturbance control was combined with the back-stepping and the SMC techniques to control unmanned tractors [17]. Fuzzy control was improved by the SMC in fault control of a double star IM [32]. Various approaches of the SMC were presented for observation and control of complex systems [35]. An Integral SMC was adjusted for sensorless IM drive using model reference adaptive system (MRAS) [38]. Proportional-integral-derivative controller was combined with the SMC to maximize IM performance [42]. The SMC using a modified exponential reaching law enhanced the induction generator control in conditions of uncertainties and disturbances [46]. In order to increase the accuracy and to lower the chattering phenomenon at control signal, the super-twisting algorithm (STA) has been combined with the SMC.

The STA was used in the controllers of primary flux-linkage and electromagnetic thrust to get not only low error, fast response of motor speed but also high robustness-to-load-variation for a linear IM system [2]. The higher order SMC and the continuous STA were combined together to stabilize the disturbed double-integrator systems [5]. An optimized neural network controller was integrated into the

adaptive STO to achieve highly precise IM drive with parameter machine uncertainties [8]. Reaching time of the multivariable STA was evaluated by the linear matrix inequality approach for the systems that have bounded parameter uncertainties and input noises [10]. Fuzzy logic was utilized in the event-triggered method of the STA-based SMC to modify the updating time for obtaining the high PMSM drive performance in case of unknown disturbances [12]. The average model of a DC voltage converter system was employed in design of the derivation of controller gains for the STA high-order SMC. Besides that, the gains were computed according to the inductor current and its disturbance boundaries to obtain high robustness to load variations [14]. To get finite time convergence of tracking errors, an integral SMC was employed for robot manipulators. The adaptive STA was also added to the SMC to provide the continuousity of control signal [16]. The SMC was combined with the MRAS technique for sensorless IM drive in case of uncertainties, and the STA was employed to minimize the chattering phenomenon in the speed controller of the drive [19]. To compensate the uncertainties and deviation caused by unbalanced load, solar irradiation and the primary layer, the gains of the STA-based SMC were adjusted by a self-tuning approach for restoration of frequency and voltage of an islanded microgrid system [20]. The STA reduced torque ripple, eliminated the high-speed switching signal in power control-based brushless motor drive system [25]. A nonlinear term was used instead of the discontinuous one in the STA, and the finite time convergence was ensured by tunining the term and gains [26]. To improve precision and increase robustness-to-parameter-variations in sensorless low-speed IM drive, the gain of the STA law was adapted using Lyapunov stability [30]. The windup effect was reduced by the conditioning method in the STA-based control law applied to servomotor control system [34]. To obtain the robustness and the finite time convergence of a quadcopter altitude control in case of load variation and ground-effect, the STA-based SMC was combined with the disturbance estimator [37]. To enhance the performance of a high-speed synchronous generator, the STA voltage controller increased anti-disturbance capability, and the STA-based load estimator was feedforward into the voltage controller to compensate [47]. To eliminate the chattering and get the fast convergence in an electromagnetic machine drive system, the STA terminal SMC was integrated into a decoupling controller for the current [48]. An STA-based tracking controller was added to ensure the stability of the mobile manipulator in case of disturbances caused by external force [49].

To increase the robustness, most of aboved STA-based SMC methods utilized additional techniques such as modified/adaptive algorithms ([2], [16], [20], [26], [30], [34], [37], [47], [48], [49]), high-order methods ([5], [14], [19], [25]), while several ones employed intelligent solutions ([8], [12]) or linear matrix inequality [10]. In next section, the PC utilizing the IM model is presented [29]. In order to design the low-chattering reference motor torque and obtain high precision in speed control, the SMC integrated STA is modified as follows: 1. Components of the disturbance term are obtained by the PC and the motor dynamic equation, 2. Boundaries of time derivative of the disturbance are set equal to the absolute value and the opposite of the absolute value of its time derivative, 3. The coefficients of the control law are chosen according to the sign of the time derivative of the disturbance. Simulations are carried out in the third section. Conclusions are shown in the final one.

2. Proposed Super-Twisting Speed Controller

Figure 1 shows the super-twisting-algorithm-based sliding mode speed controller in the induction motor predictive control. In order to compute the important quantities for the PC, the IM model is presented as follows [29]:

$$\dot{\boldsymbol{X}} = \mathbf{A}\boldsymbol{X} + \mathbf{B}\boldsymbol{v}_s, \tag{1}$$

where:

$$\boldsymbol{X} = \begin{bmatrix} \boldsymbol{i}_s \\ \boldsymbol{\psi}_r \end{bmatrix}, \tag{2}$$

$$\mathbf{A} = \begin{bmatrix} -\dfrac{L_m^2 R_r + L_r^2 R_s}{\sigma L_s L_r^2}\mathbf{I} & \dfrac{L_m R_r}{\sigma L_s L_r^2}\mathbf{I} - \dfrac{L_m n_p \omega_m}{\sigma L_s L_r}\mathbf{J} \\ \dfrac{L_m R_r}{L_r}\mathbf{I} & -\dfrac{R_r}{L_r}\mathbf{I} + n_p \omega_m \mathbf{J} \end{bmatrix}, \tag{3}$$

$$\mathbf{B}=\begin{bmatrix}\frac{1}{\sigma L_s}\mathbf{I}\\ \mathbf{0}\end{bmatrix}, \tag{4}$$

$$\sigma=1-\frac{L_m^2}{L_s L_r}, \tag{5}$$

$$\mathbf{I}=\begin{bmatrix}1 & 0\\ 0 & 1\end{bmatrix}, \mathbf{J}=\begin{bmatrix}0 & -1\\ 1 & 0\end{bmatrix}, \mathbf{0}=\begin{bmatrix}0 & 0\\ 0 & 0\end{bmatrix}, \tag{6}$$

$$\boldsymbol{v}_s=\begin{bmatrix}v_{s\alpha}\\ v_{s\beta}\end{bmatrix}, \boldsymbol{i}_s=\begin{bmatrix}i_{s\alpha}\\ i_{s\beta}\end{bmatrix}, \boldsymbol{\psi}_r=\begin{bmatrix}\psi_{r\alpha}\\ \psi_{r\beta}\end{bmatrix}, \boldsymbol{\psi}_s=\begin{bmatrix}\psi_{s\alpha}\\ \psi_{s\beta}\end{bmatrix}, \tag{7}$$

where, IM parameters and quantities include magnetizing, rotor, stator inductances L_m, L_r, L_s; rotor, stator resistances R_r, R_s; n_p: number of pole pairs; ω_m: motor speed; stator voltage, stator current, rotor flux, stator flux vectors v_s, i_s, ψ_r, ψ_s. The dynamics of the motor speed is described as follows [4]:

$$J_m\frac{d\omega_m}{dt}=T_e-T_L-B_m\omega_m, \tag{8}$$

Figure 1

Super-twisting sliding mode speed controller in predictive control of induction motor.

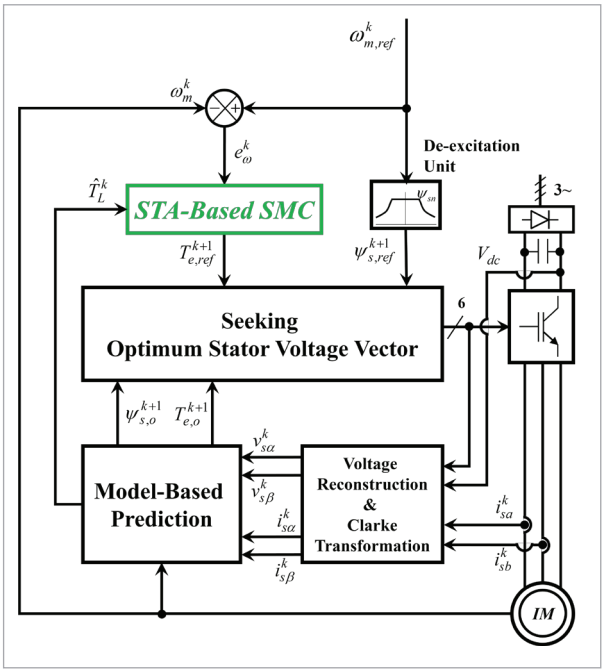

where, J_m is motor inertia, B_m is rotational viscous damping, and T_L is load torque. Motor torque T_e is computed according to following equation [4]:

$$J_m\frac{d\omega_m}{dt}=T_e-T_L-B_m\omega_m, \tag{9}$$

The motor torque and stator flux magnitude at $(k+1)^{th}$ instant, are predicted from quantities at k^{th} instant as following equations [29]:

$$\boldsymbol{\psi}^k_s=\boldsymbol{\psi}^{k-1}_s+t_c(\boldsymbol{v}^k_s-R_s\mathbf{i}^k_s), \tag{10}$$

$$\boldsymbol{\psi}^k_r=\frac{L_r}{L_m}\boldsymbol{\psi}^k_s-\frac{\sigma L_s L_r}{L_m}\boldsymbol{i}^k_s, \tag{11}$$

$$\boldsymbol{X}^{k+1}_{p,o}=\boldsymbol{X}^k+t_c\left(\mathbf{A}\boldsymbol{X}^k+\mathbf{B}\boldsymbol{v}^{k+1}_{s,o}\right), \tag{12}$$

$$\boldsymbol{X}^{k+1}_{o}=\boldsymbol{X}^{k+1}_{p,o}+\frac{t_c}{2}\mathbf{A}\left(\boldsymbol{X}^{k+1}_{p,o}-\boldsymbol{X}^k\right), \tag{13}$$

$$\boldsymbol{\psi}^{k+1}_{s,o}=\frac{L_m}{L_r}\boldsymbol{\psi}^{k+1}_{r,o}+\sigma L_s\boldsymbol{i}^{k+1}_{s,o}, \tag{14}$$

$$\psi^{k+1}_{s,o}=\left|\boldsymbol{\psi}^{k+1}_{s,o}\right|=\sqrt{\left(\psi^{k+1}_{s\alpha,o}\right)^2+\left(\psi^{k+1}_{s\beta,o}\right)^2}, \tag{15}$$

$$T^{k+1}_{e,o}=\frac{3n_p}{2}\left(\psi^{k+1}_{s\alpha,o}i^{k+1}_{s\beta,o}-\psi^{k+1}_{s\beta,o}i^{k+1}_{s\alpha,o}\right), \tag{16}$$

where: $o=1$ to 7 represents 7 stator voltage vectors of the inverter, t_c is computing period of predictive control. In Figure 1, the Seeking Optimum Stator Voltage Vector (SOSVV) block searches for the voltage vector that minimizes following cost function:

$$Z=\left|T^{k+1}_{e,ref}-T^{k+1}_{e,o}\right|+c_\psi\frac{T_{e,n}}{\psi_{s,n}}\left|\psi^{k+1}_{s,ref}-\psi^{k+1}_{s,o}\right|, \tag{17}$$

where: $T_{e,n}$ and $\psi_{s,n}$ are rated motor torque and stator flux magnitude, positive coefficient c_ψ is trial and error. Equation (16) that using stator current, stator flux components at k^{th} instant instead of $(k+1)^{th}$ instant, and Equation (8), are used to estimate the load torque at kth instant.

For design of reference motor torque, sliding mode is utilized. At first, switching function and its time derivative are defined:

$$S = \lambda e_\omega + \frac{de_\omega}{dt}, \tag{18}$$

$$\frac{dS}{dt} = \lambda \frac{d\omega_{m,ref}}{dt} - \lambda \frac{d\omega_m}{dt} + \frac{d^2 e_\omega}{dt^2}, \tag{19}$$

where: λ is a positive coeffient, $e_\omega = \omega_{m,ref} - \omega_m$. By substituting the derivative of the motor speed by Equation (8), Equation (19) is re-written as Equation (20):

$$\frac{dS}{dt} = D + u, \tag{20}$$

where, disturbance term D and control law u are respectively expressed in Equations (21) and (22):

$$D = \lambda \left(\frac{d\omega_{m,ref}}{dt} + \frac{\hat{T}_L + B_m \omega_m}{J_m} \right) + \frac{d^2 e_\omega}{dt^2}, \tag{21}$$

$$u = -\lambda \frac{T_e}{J_m}, \tag{22}$$

where: the load torque T_L at the kth instant is estimated according two Equations (10), (16) of the prediction process, and Equation (8) of the motor dynamics:

$$\hat{T}_L^k = \frac{3n_p(\psi_{s\alpha}^k i_{s\beta}^k - \psi_{s\beta}^k i_{s\alpha}^k)}{2} - B_m \omega_m^k - J_m \frac{d\omega_m^k}{dt}, \tag{23}$$

To avoid derivative kicks in computation of the time-derivative of the motor speed ω_m at the kth instant [11], transfer function of the differential term is approximated as follows:

$$G_d(s) = \frac{s}{t_c^{-1} s + 1}. \tag{24}$$

The following equation is obtained by discretizing the transfer function with sampling period t_c:

$$G_d(z) = \frac{(t_c - t_c^2) - t_c e^{-t_c^2} z^{-1}}{1 - e^{-t_c^2} z^{-1}}. \tag{25}$$

When t_c is small, the time-derivative term in Equation (23) is recursively approximated as follows:

$$\frac{d\omega_m^k}{dt} = \frac{d\omega_m^{k-1}}{dt} + (t_c - t_c^2)\omega_m^k - t_c \omega_m^{k-1}. \tag{26}$$

Lyapunov function L is defined as follows:

$$L = \frac{S^2}{2}. \tag{27}$$

In order to move the switching function to zero, the Lyapunov function must satisfy following equality:

$$\frac{dL}{dt} = S\frac{dS}{dt} \le -\kappa |S|, \tag{28}$$

where, $\kappa > 0$. The control law is selected as sign function:

$$u = -\eta sign(S), \tag{29}$$

where, $\eta > 0$. By substituting Equations (20) and (29) into Equation (28), it is converted into Equation (30):

$$\frac{dF}{dt} = SD - \eta |S| \le -\kappa |S|. \tag{30}$$

Assuming that $|D| \le M$, to satisfy the Equation (30), the coefficient η is selected as follows:

$$\eta = M + \kappa, \quad \text{for} \quad S \ne 0, \tag{31}$$

In case of the sliding mode $S = 0$, to satisfy the condition $dS/dt=0$, the control law is equal to the opposite of D. Assuming that the reference torque reaches the motor torque instantaneously, it is calculated as follows:

$$T_{e,ref} = T_e = \begin{cases} \dfrac{J_m (M + \kappa) sign(S)}{\lambda}, & \text{for } S \ne 0 \\ \dfrac{J_m D}{\lambda}, & \text{for } S = 0 \end{cases}, \tag{32}$$

For the STA SMC, the control law is modified as Equation (33):

$$u = -\eta \sqrt{|S|} sign(S). \tag{33}$$

There are two cases of the disturbance D in design of the control law. For the first case $D = 0$, substituting Equation (33) into Equation (20) leads to:

$$\frac{dS}{dt} = -\eta\sqrt{|S|}sign(S). \tag{34}$$

Equation (35) is obtained by integrating Equation (34):

$$\sqrt{|S(t)|} = \sqrt{|S_0|} - \frac{\eta}{2}t, \tag{35}$$

where, $S_0 = S(0)$. In order for the switching function to reach the sliding line $S = 0$ after time t_r, the coefficient η is chosen according to Equation (36):

$$\eta = \frac{2\sqrt{|S_0|}}{t_r}. \tag{36}$$

In the second case $D \neq 0$, it is necessary to add an auxiliary control u_a for following the disturbance D [35]:

$$u = -\eta\sqrt{|S|}sign(S) + u_a, \tag{37}$$

$$\frac{du_a}{dt} = \begin{cases} -u, \text{for } |u| > M \\ -\eta_a sign(S), \text{ for } |u| \le M \end{cases}, \tag{38}$$

where, $\eta_a > 0$. Derivative of the disturbance D is assumed to be bounded:

$$\left|\frac{dD}{dt}\right| \le F, \tag{39}$$

In case of $|u| > M$, derivative of the control law u is computed as follows:

$$\frac{du}{dt} = -\frac{1}{2}\eta\frac{dS}{dt}\frac{1}{\sqrt{|S|}} - u, \tag{40}$$

It is easy to see that:

$$u\frac{dS}{dt} = Du + u^2 > 0, \text{for } |u| > M. \tag{41}$$

Equations (40) and (41) lead to:

$$u\frac{du}{dt} = -\frac{1}{2}\eta u\frac{dS}{dt}\frac{1}{\sqrt{|S|}} - u^2 < 0, \text{for } |u| > M. \tag{42}$$

This means that the control law will go into the range $[-M, +M]$ in finite time. For case $|u| \le M$, Equation (43) is obtained by differentiating Equation (20):

$$\frac{d^2S}{dt^2} = \frac{dD}{dt} - \left(\frac{1}{2}\eta\frac{dS}{dt}\frac{1}{\sqrt{|S|}} + \eta_a sign(S)\right), \tag{43}$$

In Equation (43), d^2S/dt^2 is limited by the range:

$$\frac{d^2S}{dt^2} \in [-F, F] - \left(\frac{\eta}{2\sqrt{|S|}}\left|\frac{dS}{dt}\right| + \eta_a sign(S)\right), \tag{44}$$

In case of $S > 0$ and $dS/dt > 0$, the trajectory d^2S/dt^2 is bounded by three curves including $S = 0$, $dS/dt = 0$, and:

$$\frac{d^2S}{dt^2} = F - \eta_a. \tag{45}$$

The intersection S_I between the third and the second ones is:

$$S_I = \frac{\left(\frac{dS_0}{dt}\right)^2}{2(\eta_a - F)}. \tag{46}$$

With the proposal that upper boundary of the time derivative of the disturbance are equal to the absolute value of its time derivative: $F = |dD/dt|$, if $S > 0$ and $dS/dt < 0$, then d^2S/dt^2 is positive if and only if:

$$\begin{cases} \frac{\eta}{2\sqrt{|S|}}\left|\frac{dS}{dt}\right| > (\eta_a + F), \text{for } \frac{dD}{dt} < 0 \\ \frac{\eta}{2\sqrt{|S|}}\left|\frac{dS}{dt}\right| > (\eta_a - F), \text{for } \frac{dD}{dt} \ge 0 \end{cases}. \tag{47}$$

For $S > 0$, three curves that create main curve include:

$$\left(\frac{dS}{dt}\right)^2 = 2(\eta_a - F)(S_I - S), \quad \text{for } \frac{dS}{dt} > 0, \left(\frac{dS_0}{dt}\right)^2 = 2(\eta_a - F)S_I, \tag{48}$$

$$\begin{cases} S = S_I, \text{for } \dfrac{dD}{dt} < 0, -\dfrac{2\sqrt{S}(\eta_a + F)}{\eta} \le \dfrac{dS}{dt} \le 0 \\ S = S_I, \text{for } \dfrac{dD}{dt} \ge 0, -\dfrac{2\sqrt{S}(\eta_a - F)}{\eta} \le \dfrac{dS}{dt} \le 0 \end{cases} \quad (49)$$

$$\begin{cases} \dfrac{dS}{dt} = \dfrac{dS_I}{dt} = -\dfrac{2\sqrt{S_I}(\eta_a + F)}{\eta}, \text{for } \dfrac{dD}{dt} < 0, \\ \dfrac{dS}{dt} = \dfrac{dS_I}{dt} = -\dfrac{2\sqrt{S_I}(\eta_a - F)}{\eta}, \text{for } \dfrac{dD}{dt} \ge 0, \end{cases} \quad (50)$$

for $S_I \ge S \ge 0$

For the convergence of the STA, following condition must be satisfied:

$$\left| \frac{dS_I}{dt} \Big/ \frac{dS_0}{dt} \right| < 1. \quad (51)$$

The condition leads to Equation (52):

$$\begin{cases} \dfrac{2(\eta_a + F)^2}{\eta^2(\eta_a - F)} < 1, \text{for } \dfrac{dD}{dt} < 0 \\ \dfrac{2(\eta_a - F)}{\eta^2} < 1, \text{for } \dfrac{dD}{dt} \ge 0 \end{cases}. \quad (52)$$

The coefficients are chosen as follows:

$$\begin{cases} \eta = \left[\dfrac{\sqrt{2}(q+1)}{\sqrt{q-1}} + \varepsilon \right] \sqrt{F}, \text{for } \dfrac{dD}{dt} < 0 \\ \eta = \left[\sqrt{2(q-1)} + \varepsilon \right] \sqrt{F}, \text{for } \dfrac{dD}{dt} \ge 0 \end{cases}. \quad (53)$$

where, $\eta_a = qF$, with $q > 1$, $\varepsilon > 0$. Note that, do not take q too close to 1 and ε greater than 1 so that the n coefficient is not too large. To cope with external disturbances and machine parameters uncertainties, the ε factor is set to 0.5 by trial and error. The coefficients selection according to Equation (53) ensures that both $S \times dS/dt < 0$ and $dS/dt \times d^2S/dt^2 < 0$, that is, the stability of the system is guaranteed according to Lyapunov.

3. Simulations

Three speed controllers including the proportional-integral (PI), the conventional sliding mode (SM), the super-twisting-algorithm based sliding mode (ST) controllers, are numerically simulated in Simulink environment with t_c=2.5μs for the PC strategy of the IM drive. Time courses of reference speeds $\omega_{m,ref}$= {10rpm, 1rpm} and load torques T_L = {$0.01T_{lim}$, $0.5T_{lim}$, $0.99T_{lim}$} are shown in Figures 2 and 3. In Figure 2, there are 3 durations when the reference speed changes linearly: 0s-0.1s (from 0 to $\omega_{m,ref}$), 1.2s-1.4s (from $\omega_{m,ref}$ to $-\omega_{m,ref}$), 2.5s-2.6s (from $-\omega_{m,ref}$ to 0), and the reference one is constant in the remaining intervals: 0.1s-1.2s, 1.4s-2.5s, 2.6s-3.0s. Figure 3 contains 4 variable-load-torque durations: 0.4s-0.5s (from 0 to T_L), 0.8s-0.9s (from T_L to 0), 1.6s-1.7s (from 0 to $-T_L$), 2.0s-2.1s (from $-T_L$ to 0), and 5 constant-load-torque ones: 0.0s-0.4s, 0.5s-0.8s, 0.9s-1.6s, 1.7s-2.0s, 2.1s-3.0s. Parameters of the motor and the speed controllers are respectively listed in Tables 1 and 2.

Figures 4-9 show speed responses for all simulated cases. It can be easy to see that in cases T_L = {$0.5T_{lim}$, $0.99T_{lim}$} (see Figures 5, 6, 8, and 9) the PI owns greatest undershoot or overshoot at times when load torque changes (0.4s, 0.8s, 1.6s, and 2.0s). In Figures 4-9, their enlarged images indicate that the ST responds fastest to changes of the reference speed or load torque, and gives highest tracking accuracy. Two performance indices including relative final error (RFE) and normalized integral time absolute error (NITAE) of the motor speed are utilized to evaluate three controllers:

$$NITAE = \frac{\int_0^3 t\left|e_\omega(t)\right| dt}{\omega_{m,ref}}. \quad (54)$$

The RFE values at 7 times: 0.4s, 0.8s, 1.2s, 1.6s, 2s, 2.5s, and 3s, are respectively listed in Tables 3-9. The RFE for ST is many times smaller than that for PI, and usually the larger the load, the larger the difference between two controllers. In the cases T_L = {$0.5T_{lim}$, $0.99T_{lim}$}, the RFE for SM is approximately equal or several times higher than that for ST. The NITAE values in Table 10 show the speed control accuracy of the ST compared to the SM and the PI

over the entire time courses. Compared with PI, it decreases the NITAE value by more than 99%, especially at $T_L = 0.99T_{lim}$ the reduction is over 99.9%. The ST also lowers 18.3%-39.8% and 66.7%-89.6% of the NITAE compared to the SM at $\omega_{m,ref}$ = 10rpm and $\omega_{m,ref}$ = 1rpm, respectively.

Table 1
Motor parameters [38].

Quantity	Symbol	Value
Magnetizing inductance	L_m	0.192H
Rotor and stator inductances	$L_r = L_s$	0.209H
Rotor resistance	R_r	2.118Ω
Stator resistance	R_s	3.179Ω
Number of pole pairs	n_p	2
Rated motor speed	$\omega_{m,n}$	1420rpm
Motor inertia	J_m	0.0047kg·m^2
Rated motor torque	$T_{e,n}$	14.8N·m
Rated stator flux magnitude	$\psi_{s,n}$	0.78Wb
Rated motor power	P_n	2.2kW

Table 2
Speed controller parameters [38].

Controller	Quantity	Value
PI	Proportional gain K_p	1.5N·m/rpm
PI	Integral time constant T_i	0.05s
PI, SM, ST	Limitations of reference output torque T_{lim}	±10N·m
SM, ST	λ	1000
ST	q	1.1
ST	ε	0.5

Figure 2
Reference speeds: $\omega_{m,ref}$ = 10rpm (upper) and $\omega_{m,ref}$ = 1rpm (lower).

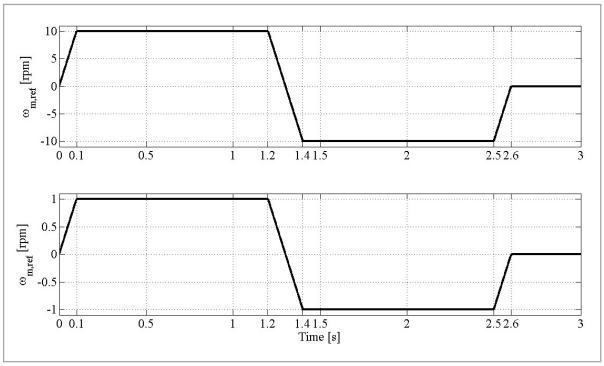

Figure 3
Load torques: $T_L = 0.01T_{lim}$ (upper), $T_L = 0.5T_{lim}$ (middle), $T_L = 0.99T_{lim}$ (lower).

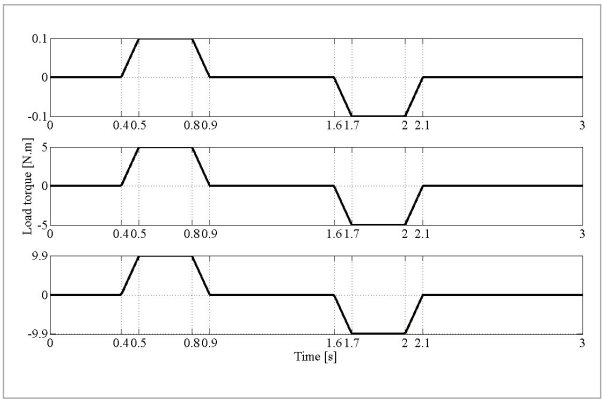

Figure 4
Speed responses at $T_L = 0.01T_{lim}$, $\omega_{m,ref}$ = 10rpm.

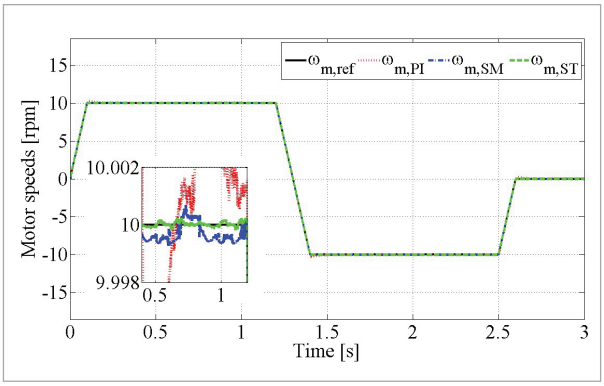

Figure 5
Speed responses at $T_L = 0.5T_{lim}$, $\omega_{m,ref}$ = 10rpm.

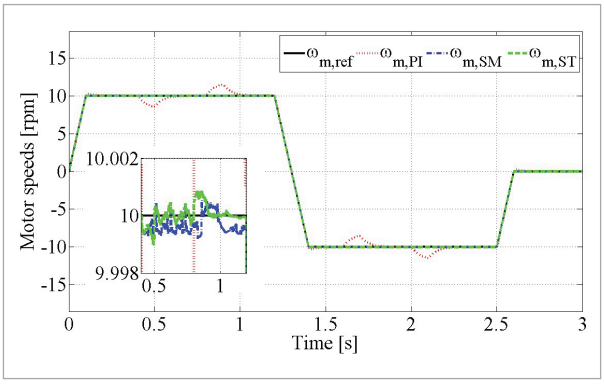

Figure 6

Speed responses at $T_L = 0.99T_{lim}$, $\omega_{m,ref} = 10$rpm.

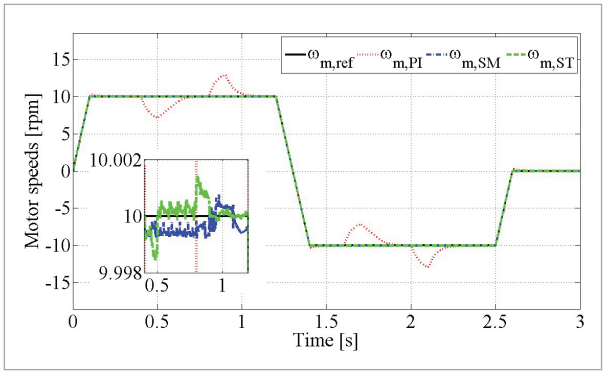

Figure 7

Speed responses at $T_L = 0.01T_{lim}$, $\omega_{m,ref} = 1$rpm.

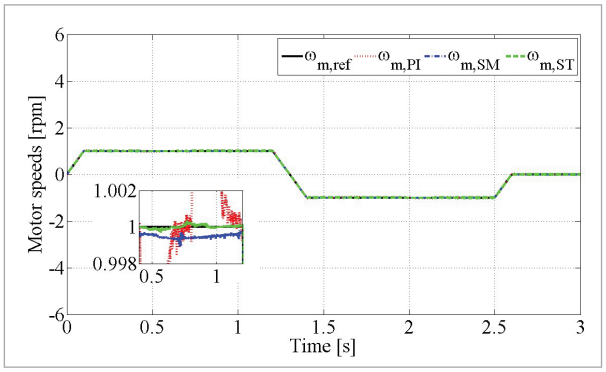

Figure 8

Speed responses at $T_L = 0.5T_{lim}$, $\omega_{m,ref} = 1$rpm.

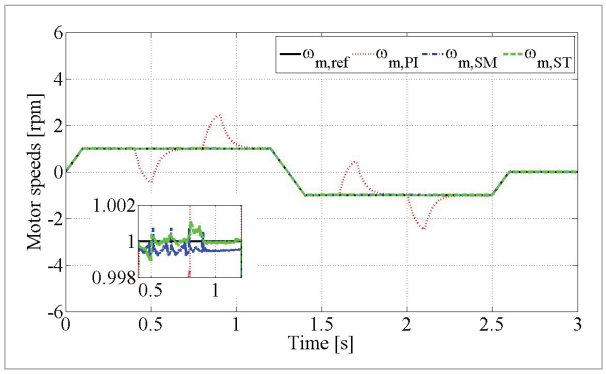

Figure 9

Speed responses at $T_L = 0.99T_{lim}$, $\omega_{m,ref} = 1$rpm.

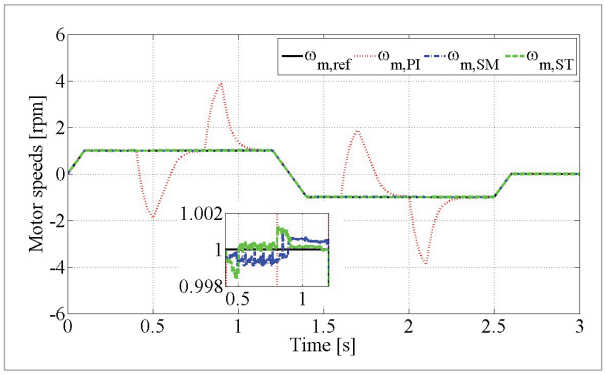

Table 3

RFE value at 0.4s [$\times 10^{-4}$].

$\omega_{m,ref}$	PI	SM	ST
10 rpm	1.82	0.33	0.012
1 rpm	4.02	3.20	0.044

Table 4

RFE value at 0.8s [$\times 10^{-4}$].

T_L	$\omega_{m,ref}$ = 10 rpm			$\omega_{m,ref}$ = 1 rpm		
	PI	SM	ST	PI	SM	ST
$0.01T_{lim}$	1.31	0.24	0.014	4.98	5.84	1.56
$0.5T_{lim}$	2.74	0.35	0.13	17.22	3.51	3.54
$0.99T_{lim}$	15.99	0.51	0.30	153.2	7.24	1.74

Table 5

RFE value at 1.2s [$\times 10^{-4}$].

T_L	$\omega_{m,ref}$ = 10 rpm			$\omega_{m,ref}$ = 1 rpm		
	PI	SM	ST	PI	SM	ST
$0.01T_{lim}$	1.54	0.081	0.12	3.87	3.49	1.11
$0.5T_{lim}$	2.11	0.45	0.045	22.8	4.71	0.78
$0.99T_{lim}$	7.11	0.36	0.044	49.2	3.73	0.092

Table 6

RFE value at 1.6s [$\times 10^{-4}$].

T_L	$\omega_{m,ref}$ = 10 rpm			$\omega_{m,ref}$ = 1 rpm		
	PI	SM	ST	PI	SM	ST
$0.01T_{lim}$	2.66	0.54	0.0078	8.67	5.19	0.41
$0.5T_{lim}$	6.37	0.57	0.11	8.07	5.5	0.52
$0.99T_{lim}$	5.93	0.58	0.0016	5.95	6.21	1.36

Table 7
RFE value at 2s [×10^{-4}].

T_L	$\omega_{m,ref}$ = 10 rpm			$\omega_{m,ref}$ = 1 rpm		
	PI	SM	ST	PI	SM	ST
$0.01T_{lim}$	5.39	0.20	0.077	4.74	3.70	1.08
$0.5T_{lim}$	2.24	0.56	0.31	24.73	5.99	1.36
$0.99T_{lim}$	16.38	0.54	0.19	161.0	4.71	0.14

Table 8
RFE value at 2.5s [×10^{-4}].

T_L	$\omega_{m,ref}$ = 10 rpm			$\omega_{m,ref}$ = 1 rpm		
	PI	SM	ST	PI	SM	ST
$0.01T_{lim}$	2.56	0.29	0.11	9.66	4.60	0.52
$0.5T_{lim}$	2.44	0.33	0.10	20.0	4.63	0.037
$0.99T_{lim}$	1.38	0.22	0.15	26.62	4.98	0.48

Table 9
RFE value at 3s [×10^{-4}].

T_L	$\omega_{m,ref}$ = 10 rpm			$\omega_{m,ref}$ = 1 rpm		
	PI	SM	ST	PI	SM	ST
$0.01T_{lim}$	0.21	0.43	0.01	2.61	4.87	0.033
$0.5T_{lim}$	0.50	0.54	0.036	7.59	4.86	0.032
$0.99T_{lim}$	1.21	0.44	0.035	2.11	5.30	0.075

Table 10
NITAE value [×10^{-3}s^2].

T_L	$\omega_{m,ref}$ = 10 rpm			$\omega_{m,ref}$ = 1 rpm		
	PI	SM	ST	PI	SM	ST
$0.01T_{lim}$	13.8	0.19	0.11	30.5	2.11	0.22
$0.5T_{lim}$	98.9	0.20	0.15	880.9	2.08	0.49
$0.99T_{lim}$	209.0	0.21	0.17	1979.0	2.24	0.74

Figures 10-12 show speed errors for the SM and ST controllers. They indicate that after the speed error of the ST is suddenly changed by the variations of the reference speed or the load torque, it returns much closer to zero than that of the PI and the SM. The explanation for this is the output signal-the reference torque of the PI does not adapt to changes of load torque or reference speed, while the output one of the SM is always switched to $\pm T_{lim}$ even though the load torque is only $0.01T_{lim}$ (see Figure 13). Meanwhile, the ST gives the reference torque with much smaller oscillation than the SM, comparable to the PI at all cases of the load torque (see Figures 14-16). In Figures 17-19, the switching function for the ST contains more constant segments and lower chattering than that for the SM because in case of the ST, both S and dS/dt are designed to achieve $S = dS/dt = 0$.

Figure 10
Speed errors at $T_L = 0.01T_{lim}$, $\omega_{m,ref}$ = 10rpm (upper) and $\omega_{m,ref}$ = 1rpm (lower).

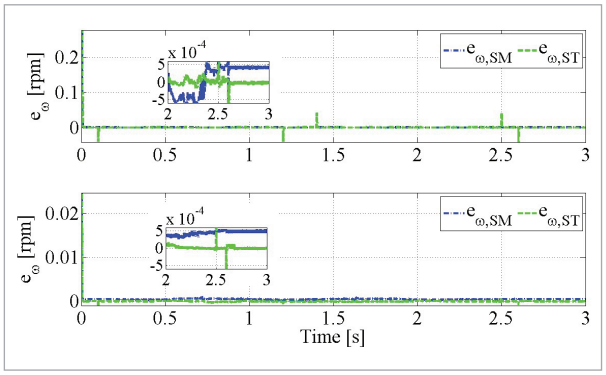

Figure 11
Speed errors at $T_L = 0.5T_{lim}$, $\omega_{m,ref}$ = 10rpm (upper) and $\omega_{m,ref}$ = 1rpm (lower).

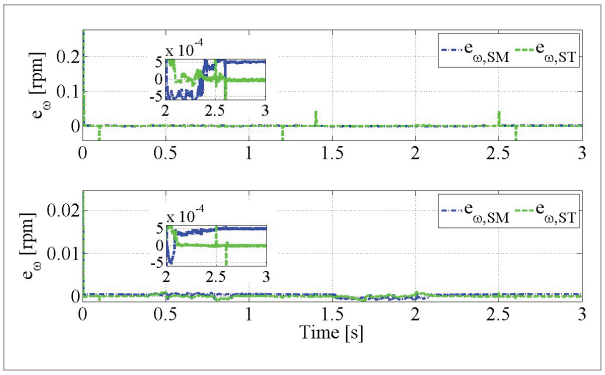

Figure 12

Speed errors at $T_L = 0.99T_{lim}$, $\omega_{m,ref}$= 10rpm (upper) and $\omega_{m,ref}$= 1rpm (lower).

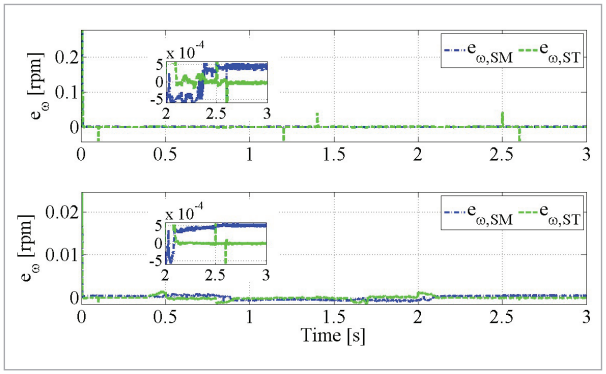

Figure 13

Reference torque-output of the SM at $T_L = 0.01T_{lim}$, $\omega_{m,ref}$ = 10rpm (upper) and $\omega_{m,ref}$ = 1rpm (lower).

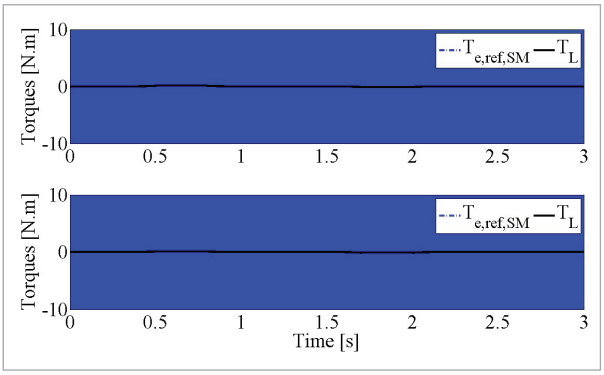

Figure 14

Reference torques-outputs of the ST and the PI at T_L = $0.01T_{lim}$, $\omega_{m,ref}$ = 10rpm (upper) and $\omega_{m,ref}$ = 1rpm (lower).

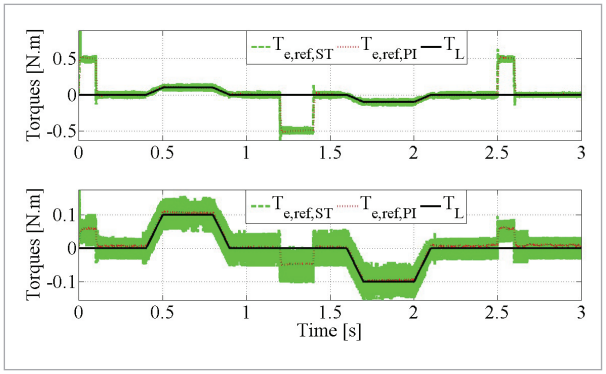

Figure 15

Reference torques-outputs of the ST and the PI at T_L = $0.5T_{lim}$, $\omega_{m,ref}$ = 10rpm (upper) and $\omega_{m,ref}$ = 1rpm (lower).

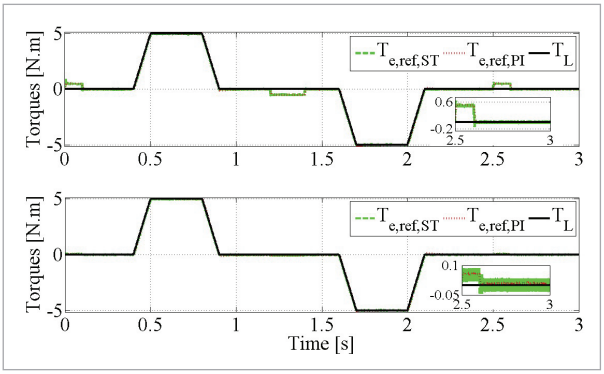

Figure 16

Reference torques-outputs of the ST and the PI at T_L = $0.99T_{lim}$, $\omega_{m,ref}$ = 10rpm (upper) and $\omega_{m,ref}$= 1rpm (lower).

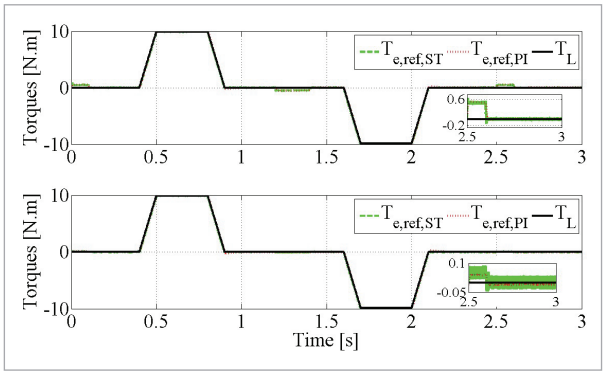

Figure 17

Switching functions of the SM and the ST at $T_L = 0.01T_{lim}$, $\omega_{m,ref}$ = 10rpm (upper) and $\omega_{m,ref}$= 1rpm (lower).

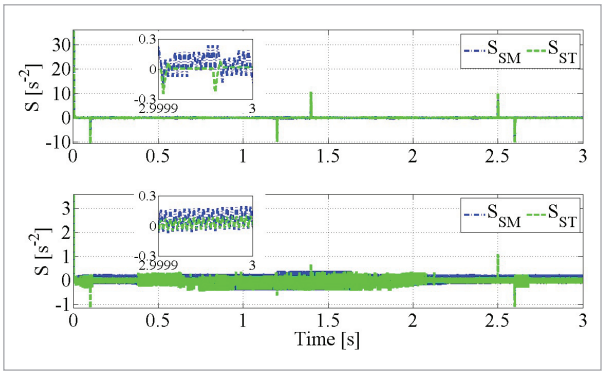

Figure 18
Switching functions of the SM and the ST at $T_L = 0.5T_{lim}$, $\omega_{m,ref}$ = 10rpm (upper) and $\omega_{m,ref}$ = 1rpm (lower).

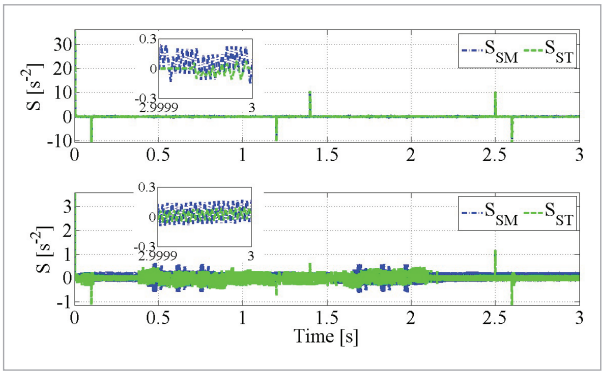

Figure 19
Switching functions of the SM and the ST at $T_L = 0.99T_{lim}$, $\omega_{m,ref}$ = 10rpm (upper) and $\omega_{m,ref}$ = 1rpm (lower).

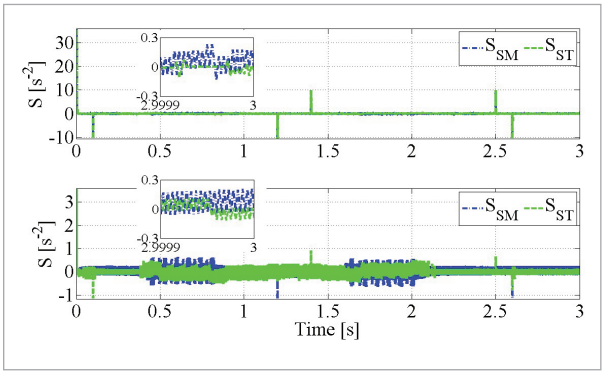

4. Conclusions and Developments

The ST and the SM were presented and simulated at very-low reference speeds and wide load torque range in the IM predictive control. The ST provides higher accurate speed control than both the PI and SM, the reductions in the NITAE index up to 99.9% and 89.6%, respectively. The chattering phenomenon at the control signal of the conventional SMC is eliminated almost completely by the proposed STA. The trajectories of the switching function and its time derivative in the SM are much closer to zero than the SM. Sophiscated STA designs such as multivariable systems [27] or strict Lyapunov function [28] can be used to approach the trajectories to zero. Modified PC methods can be employed to reduce computing requirements. In order to obtain accurate information of the motor speed, parameters and the disturbances, high-performance observers integrating higher-order sliding mode or adaptive method can be utilized [5], [13]. The proposed STA can be applied to some types of motors such as permanent magnet synchronous motor, brushless DC motor or industrial systems whose models are predictable and whose disturbances can be estimated. A model hardware using a high-speed digital signal processor-based control system can be deployed to validate practical feasibility and robustness of the proposed controller [7], [19].

References

1. Accetta, A., Cirrincione, M., D'Ippolito, F., Pucci, M., Sferlazza, A. Input-Output Feedback Linearization Control of a Linear Induction Motor Taking into Consideration Its Dynamic End-Effects and Iron Losses. IEEE Transactions on Industry Applications, 2022, 58(3), 3664-3673. https://doi.org/10.1109/TIA.2022.3160409
2. Ali, M. M., Xu, W., Junejo, A. K., Elmorshedy, M. F., Tang, Y. One New Super-Twisting Sliding Mode Direct Thrust Control for Linear Induction Machine Based on Linear Metro. IEEE Transactions on Power Electronics, 2022, 37(1), 795-805. https://doi.org/10.1109/TPEL.2021.3096066
3. Brandstetter, P., Krna, P. Sensorless control of switched reluctance motor using sliding mode observer. 2013 International Conference on Applied Electronics, Pilsen, Czech Republic, 2013, 1-4.
4. Bose, B. K. Modern Power Electronics and AC Drives, ch. 8. Prentice Hall, New Jersey, 2002.
5. Chalanga, A., Kamal, S., Fridman, L. M., Bandyopadhyay, B., Moreno, J. A. Implementation of Super-Twisting Control: Super-Twisting and Higher Order Sliding-Mode Observer-Based Approaches. IEEE Transactions on Industrial Electronics, 2016, 63(6), 3677-3685. https://doi.org/10.1109/TIE.2016.2523913

6. Chantoufi, A., Derouich, A., Ouanjli, N. E., Mahfoud, S., Idrissi, A. E., Tazay, A. F. Direct Torque Control-Based Backstepping Speed Controller of Doubly Fed Induction Motors in Electric Vehicles: Experimental Validation. IEEE Access, 2024, 12, 139758-139772. https://doi.org/10.1109/ACCESS.2024.3462821
7. Dong, C. S. T., Vo, H. H., Tran, T. C., Brandstetter, P., Simonik, P. Application of Sensorless Sliding Mode Observer in Control of Induction Motor Drive. Advances in Electrical and Electronic Engineering, 2017, 15(5), 747-753. https://doi.org/10.15598/aeee.v15i5.2626
8. El-Sousy, F. F. M., Amin, M. M., Mohammed, O. A. Robust Adaptive Neural Network Tracking Control with Optimized Super-Twisting Sliding-Mode Technique for Induction Motor Drive System. IEEE Transactions on Industry Applications, 2022, 58(3), 4134-4157. https://doi.org/10.1109/TIA.2022.3160136
9. Elmorshedy, M. F., Xu, W., Almakhles, D., Kotb, K. M. Reduced Flux Ripples for Linear Induction Machines Based-Two Voltage Vectors Finite State Model Predictive Control with MTPA. 2023 IEEE International Conference on Predictive Control of Electrical Drives and Power Electronics (PRECEDE), Wuhan, China, 2023, 1-6. https://doi.org/10.1109/PRECEDE57319.2023.10174498
10. Geromel, J. C., Hsu, L., Nunes, E. V. L. On Multivariable Super-Twisting Algorithm Reaching Time Assessment. IEEE Transactions on Automatic Control, 2024, 69(11), 7972-7979. https://doi.org/10.1109/TAC.2024.3407018
11. Gopal, M. Digital Control and State Variable Methods, ch. 3. Tata McGraw-Hill, New Delhi, 2003.
12. Gu, J., You, S., Kim, W., Moon, J. Fuzzy Event-Triggered Super Twisting Sliding Mode Control for Position Tracking of Permanent Magnet Synchronous Motors Under Unknown Disturbances. IEEE Transactions on Industrial Informatics, 2023, 19(9), 9843-9854. https://doi.org/10.1109/TII.2022.3231410
13. Hassen, M. D., Laamiri, I., Bouguila, N. A Robust Adaptive Non-Singular Terminal Sliding Mode Control: Application to an Upper-Limb Exoskeleton with Disturbances and Uncertain Dynamics. Information Technology and Control, 2024, 53(1), 171-186. https://doi.org/10.5755/j01.itc.53.1.33752
14. Hatlehol, M. U., Zadeh, M. Super-Twisting Algorithm Second-Order Sliding Mode Control of a Bidirectional DC-to-DC Converter Supplying a Constant Power Load. IFAC-PapersOnLine, 2022, 55(31), 287-294. https://doi.org/10.1016/j.ifacol.2022.10.444
15. He, L., He, H., Zuo, K., Davronbekov, D. A., Wang, F. Efficiency Optimal Predictive Control of Induction Motor Based on Loss Model Method. 2023 26th International Conference on Electrical Machines and Systems (ICEMS), Zhuhai, China, 2023, 2113-2118. https://doi.org/10.1109/ICEMS59686.2023.10345139
16. Hu, J., Zhang, X., Zhang, D., Chen, Y., Ni, H., Liang, H. Finite-time adaptive super-twisting sliding mode control for autonomous robotic manipulators with actuator faults. ISA Transactions, 2024, 144, 342-351. https://doi.org/10.1016/j.isatra.2023.10.028
17. Ji, X., Wei, X., Wang, A. A Novel Control Method for Unmanned Agricultural Tractors: Composite Back-stepping Sliding Mode Path Tracking. Information Technology and Control, 2023, 52(2), 515-528. https://doi.org/10.5755/j01.itc.52.2.31649
18. Kozubik, M., Vesely, L., Aufderheide, E., Vaclavek, P. Parallel Computing Utilization in Nonlinear Model Predictive Control of Permanent Magnet Synchronous Motor. IEEE Access, 2024, 12, 128187-128200. https://doi.org/10.1109/ACCESS.2024.3456432
19. Krim, S., Mimouni, M. F. Design and Xilinx Virtex-field-programmable gate array for hardware in the loop of sensorless second-order sliding mode control and model reference adaptive system-sliding mode observer for direct torque control of induction motor drive. Proceedings of the Institution of Mechanical Engineers, Part I: Journal of Systems and Control Engineering, 2023, 237(5), 839-869. https://doi.org/10.1177/09596518221138987
20. Kumar Panda, S., Subudhi, B. A Distributed Adaptive Super-Twisting Sliding Mode Controller for Voltage and Frequency Restoration in Islanded Microgrid. IEEE Journal of Emerging and Selected Topics in Power Electronics, 2025, 13(1), 1010-1017. https://doi.org/10.1109/JESTPE.2024.3468152
21. Li, S., Zhang, J., Li, M., Wu, F., Zhou, P. Disturbance Observer-Based Neural Adaptive Command Filtered BacksStepping Funnel-Like Control for the Chaotic PMSM With Asymmetric Prescribed Performance Constraints. International Journal of Robust and Nonlinear Control, 2025, 35(3), 1183-1200. https://doi.org/10.1002/rnc.7712
22. Li, Y., Miao, Z., Zhang, L., Zhang, H. Application of Finite Set Model Predictive Control to Five-Phase Induction Motors. 2023 5th International Conference on Electrical Engineering and Control Technologies (CEECT), Chengdu, China, 2023, 469-473. https://doi.org/10.1109/CEECT59667.2023.10420762

23. Long, B., Shen, D., Cao, T., Rodriguez, J., Garcia, C., Guerrero, J. M. Power Losses Reduction of T-Type Grid-Connected Converters Based on Tolerant Sequential Model Predictive Control. IEEE Transactions on Power Electronics, 2022, 37(8), 9089-9103. https://doi.org/10.1109/TPEL.2022.3157341

24. Luo, Y., Yang, K., Zheng, Y. Feedback Linearization-Based Direct Torque Control for Asymmetrical Six-Phase PMSM Motor with Back EMF Harmonics Compensation. IEEE Journal of Emerging and Selected Topics in Power Electronics, 2023, 11(5), 5145-5155. https://doi.org/10.1109/JESTPE.2023.3292922

25. Masoudi, H., Kiyoumarsi, A., Madani, S. M., Ataei, M. Torque Ripple Reduction of Nonsinusoidal Brushless DC Motor Based on Super-Twisting Sliding Mode Direct Power Control. IEEE Transactions on Transportation Electrification, 2023, 9(3), 3769-3779. https://doi.org/10.1109/TTE.2023.3250950

26. Mei, K., Ding, S., Yu, X. A Generalized Supertwisting Algorithm. IEEE Transactions on Cybernetics, 2023, 53(6), 3951-3960. https://doi.org/10.1109/TCYB.2022.3188877

27. Moreno, J. A., García-Mathey, J. F. MIMO Super-Twisting Controller using a passivity-based design, Journal of the Franklin Institute, 2024, 361(17), 107296. https://doi.org/10.1016/j.jfranklin.2024.107296

28. Moreno, J. A., Osorio, M. Strict Lyapunov Functions for the Super-Twisting Algorithm. IEEE Transactions on Automatic Control, 2012, 57(4), 1035-1040. https://doi.org/10.1109/TAC.2012.2186179

29. Nguyen, D. Q., Vo, H. H. Induction Motor Drive Using Model Prediction Torque Control. From Smart City to Smart Factory for Sustainable Future: Conceptual Framework, Scenarios, and Multidiscipline Perspectives, Lecture Notes in Networks and Systems, 2024, 1062, 89-96. https://doi.org/10.1007/978-3-031-65656-9_9

30. Nurettin, A., Inanc, N. Sensorless Vector Control for Induction Motor Drive at Very Low and Zero Speeds Based on an Adaptive-Gain Super-Twisting Sliding Mode Observer. IEEE Journal of Emerging and Selected Topics in Power Electronics, 2023, 11(4), 4332-4339. https://doi.org/10.1109/JESTPE.2023.3265352

31. Rigatos, G. G., Siano, P., Al-Numay, M. S., Sari, B., Abbaszadeh, M. Nonlinear optimal control for the five-phase induction motor-based traction system of electric vehicles. COMPEL - The international journal for computation and mathematics in electrical and electronic engineering, 2024, 43(1), 167-191. https://doi.org/10.1108/COMPEL-05-2023-0186

32. Said, Z., Abdelhafidh, M. Current sensor fault tolerant control of a double star induction motor DSIM using fuzzy sliding control. 2023 International Conference on Electrical Engineering and Advanced Technology (ICEEAT), Batna, Algeria, 2023, 1-6. https://doi.org/10.1109/ICEEAT60471.2023.10426182

33. Santos, T. B. D., Oliani, I., Figueiredo, R., Albieiro, D., Pelizari A., Sguarezi Filho, A. J. Robust Finite Control Set Model Predictive Current Control for Induction Motor Using Deadbeat Approach in Stationary Frame. IEEE Access, 11, 13067-13078, 2023. https://doi.org/10.1109/ACCESS.2022.3223385

34. Seeber, R., Reichhartinger, M. Conditioned Super-Twisting Algorithm for systems with saturated control action. Automatica, 2020, 116, 108921. https://doi.org/10.1016/j.automatica.2020.108921

35. Shtessel, Y., Edwards, C., Fridman, L., Levant, A. Sliding Mode Control and Observation. Springer, New York, 2014. https://doi.org/10.1007/978-0-8176-4893-0

36. Sivadharshini, A., Nguyen, N. D., Lee, Y. I. Model Predictive Current Control for Grid-connected Inverter Considering the PLL Dynamics. International Journal of Control, Automation and Systems, 2024, 22(11), 3255-3265. https://doi.org/10.1007/s12555-023-0849-x

37. Smith, S., Pan, Y. -J. Adaptive Observer-Based Super-Twisting Sliding Mode Control for Low Altitude Quadcopter Grasping. IEEE/ASME Transactions on Mechatronics, 2025, 30(1), 587-598. https://doi.org/10.1109/TMECH.2024.3400871

38. Vo, H. H. Sensorless Induction Motor Drive Using Modified Integral Sliding Mode Control-Based MRAS. Control Engineering and Applied Informatics, 2023, 25(3), 45-54. https://doi.org/10.61416/ceai.v25i3.8563

39. Wang, B., Iwasaki, M., Yu, J. Command Filtered Adaptive Backstepping Control for Dual-Motor Servo Systems with Torque Disturbance and Uncertainties. IEEE Transactions on Industrial Electronics, 2022, 69(2), 1773-1781. https://doi.org/10.1109/TIE.2021.3059540

40. Wang, Z., She, J., Sato, D., Kawata, S. Robust Disturbance-Rejection Design for Systems with Uncertainties, Disturbances, and Noise. IEEE Transactions on Industrial Informatics, 2025, 21(3), 2134-2143. https://doi.org/10.1109/TII.2024.3495754

41. Wu, Q., Sun, N., Yang, T., Fang, Y. Deep Reinforcement Learning-Based Control for Asynchronous Motor-Actuated Triple Pendulum Crane Systems with Distributed Mass Payloads. IEEE Transactions on Indus-

trial Electronics, 2024, 71(2), 1853-1862. https://doi.org/10.1109/TIE.2023.3262891

42. Yadav, A., Das, R., Roy, G. PID-Based Nonlinear Sliding Mode Control for Speed Regulation in Induction Motors: A Comprehensive Survey and Analysis. 2024 IEEE International Students' Conference on Electrical, Electronics and Computer Science (SCEECS), Bhopal, India, 2024, 1-7. https://doi.org/10.1109/SCEECS61402.2024.10482307
43. Yang, G., Yao, J. Multilayer neurocontrol of high-order uncertain nonlinear systems with active disturbance rejection. International Journal of Robust and Nonlinear Control, 2024, 34(4), 2972-2987. https://doi.org/10.1002/rnc.7118
44. Yang, G. State filtered disturbance rejection control. Nonlinear Dynamics, 2025, 113(7), 6739-6755. https://doi.org/10.1007/s11071-024-10449-6
45. Yang, Q., Karamanakos, P., Liegmann, E., Tian, W., Geyer, T., Kennel, R. A Fixed Switching Frequency Direct Model Predictive Control for Neutral-Point-Clamped Three-Level Inverters with Induction Machines. IEEE Transactions on Power Electronics, 2023, 38(11), 13703-13716. https://doi.org/10.1109/TPEL.2023.3300098
46. Yang, Y., Xie, W. Speed Control of Doubly-Fed Induction Generator Based on a Improved Reaching Law Integral Sliding Mode Structure. 2023 4th International Conference on Advanced Electrical and Energy Systems (AEES), Shanghai, China, 2023, 264-269. https://doi.org/10.1109/AEES59800.2023.10469550
47. Yin, S., Wang, X. Super Twisting Control Design for HSPMSG Voltage Stabilization Based on Disturbance Observation Compensation. IEEE Transactions on Energy Conversion, 2023, 38(2), 1387-1395. https://doi.org/10.1109/TEC.2022.3215509
48. Yu, X., Zhou, B., Fang, W., Jiang, S., Zhou, X., Xiong, L. Super-Twisting Terminal Sliding Mode Decoupling Current Control for Sinusoidal Doubly Salient Electromagnetic Machine Drives. IEEE Transactions on Energy Conversion, 2025, 40(1), 106-122. https://doi.org/10.1109/TEC.2024.3424503
49. Zhang, S., Cheng, S., Jin, Z. Variable Trajectory Impedance: A Super-Twisting Sliding Mode Control Method for Mobile Manipulator Based on Identification Model. IEEE Transactions on Industrial Electronics, 2025, 72(1), 610-619. https://doi.org/10.1109/TIE.2024.3383042